RSC Advances

PAPER

View Article Online
View Journal | View Issue

Cite this: *RSC Adv.*, 2026, **16**, 11897

Green synthesis of high-performance CHA zeolite membranes in pure K^+ clear solution

Chuncheng Li,[a] Zijian Zhang,[a] Chunwei Yang *[a] and Pengfei Wang*[ab]

Received 4th January 2026
Accepted 18th February 2026

DOI: 10.1039/d6ra00071a

rsc.li/rsc-advances

CHA zeolite membranes possess a unique microporous structure and excellent hydrothermal stability, making them ideal materials for efficient dehydration of organic solvents. In this study, CHA zeolite membranes with SiO_2/Al_2O_3 ratios of 3.6–5.4 were successfully synthesized on α-Al_2O_3 supports using a high water-to-silica ratio (H_2O/SiO_2 = 230) system, using K^+ as the structure-directing agent. The effects of the seed crystals' SiO_2/Al_2O_3 ratio and concentration, as well as the hydrothermal temperature, on the membrane microstructure and performance were systematically investigated. Particular emphasis was placed on elucidating the regulatory mechanism of seed properties and synthesis conditions on membrane growth. Low SiO_2/Al_2O_3 ratio seeds promoted the formation of prismatic crystals with sizes of 2–4 μm, whereas high ratios tended to generate impurity phases, which worsened with increasing concentration. Ultimately, under optimal conditions of a seed SiO_2/Al_2O_3 ratio of 4.84, seed concentration of 3 wt%, and synthesis temperature of 150 °C, the resulting CHA membrane exhibited outstanding pervaporation performance. For a 90 wt% ethanol/water solution (75 °C), the separation factor was as high as 5800, with a flux of 10.6 kg m^{-2} h^{-1}. For a 40 wt% acetic acid/water solution, the permeate water content remained above 98.95%, with a flux of 4.8 kg m^{-2} h^{-1}.

1. Introduction

Organic solvents are widely used in petrochemical processing, biopharmaceutical production, and polymer synthesis.[1–3] However, dehydration of organic solvents typically relies on conventional techniques such as distillation and adsorption, which are characterized by high energy consumption, significant waste generation, and poor economic efficiency. These limitations are particularly severe in azeotropic systems, where the separation efficiency is low and complete water removal is difficult to achieve.[4–6] Therefore, the development of pervaporation (PV) dehydration processes with lower energy requirements and higher efficiency represents an important direction for future solvent separation technologies.[7] Membrane materials play a decisive role in determining separation performance. Compared with organic membranes, zeolite membranes are composed of inorganic frameworks with uniform pore structures and exhibit negligible swelling in organic solvents. This endows them with superior chemical resistance, thermal stability, and stable separation performance in water/organic solvent systems.[8,9]

In recent years, various zeolite membranes, such as CHA,[10–12] LTA,[13,14] NaY,[15,16] T,[17,18] MOR,[19,20] and ZSM-5 (ref. 21 and 22) have been developed for organic solvent dehydration. Among them, LTA zeolite membranes have shown excellent performance in alcohol–water separation and have been implemented industrially. Nevertheless, their relatively low acid and hydrothermal stability severely restricts further application.[23] CHA-type zeolites consist of a three-dimensional framework of large cage structures (6.7 Å × 10 Å) interconnected by eight-membered-ring windows (3.8 Å × 3.8 Å). The pore size (3.8 Å) closely matches the kinetic diameter of water molecules (2.7 Å), resulting in excellent molecular sieving selectivity toward water. Consequently, CHA zeolite membranes exhibit outstanding PV performance. Furthermore, due to their higher SiO_2/Al_2O_3 ratios (2–∞), CHA membranes possess much greater hydrothermal and acid stability than LTA membranes, offering significant potential for industrial application.[24] Currently, most hydrophilic (low/medium silica) CHA zeolite membranes used for dehydration are synthesized *via* OSDA-free routes, typically employing alkali metal cations (*e.g.*, Na^+, K^+) or ions such as cesium, strontium, and fluorine as inorganic structural directing agents.[25] For high-silica CHA zeolite membranes, organic template agents remain necessary at present. However, the use of toxic and expensive organic structure-directing agents or the addition of reagents containing strontium, cesium, fluorine, and other elements inevitably leads to increased production costs and a series of environmental protection issues.[26,27] Therefore, considering the use of readily available alkali metal cations as inorganic structural directing agents for

[a]*Shanghai Luqiang New Materials Co., Ltd, Shanghai, 201806, P. R. China. E-mail: yang664686@163.com; wpf@sh-lq.com*

[b]*State Key Laboratory of Polyolefins and Catalysis, Shanghai Research Institute of Chemical Industry CO., Ltd, Shanghai, 200062, P. R. China*

preparing CHA zeolite membranes undoubtedly represents a more economical and green synthetic route.

Meanwhile, extensive research has demonstrated that the state of precursors significantly influences zeolite membrane growth. Compared to gels, clear solutions with lower viscosity can synthesize thinner zeolite membranes with superior PV performance.[28–33] However, most research either uses Na^+ or Na^+/K^+ mixed alkali.[12,34,35] Notably, in this system, the addition of Na^+—even in small amounts—weakens the stable negatively charged double layer of the aluminosilicate solvent, leading to the formation of a gel-like precursor. This results in thicker, lower-performance CHA zeolite films (Fig. S1). Therefore, we employed K^+ as the sole alkali metal cation and SDA, and explore the regulation of seed type (low-silica chabazite *vs.* high-silica SSZ-13), seed concentration and crystallization temperature on CHA zeolite membrane structure in a transparent synthetic solution system, and screen the synthesis conditions with high permeation flux and high separation selectivity, which provides theoretical support for the green preparation of CHA zeolite membrane.

2. Experimental

2.1 Chemicals and materials

KOH (AR, Sinopharm Chemical Reagent Co., Ltd), $Al(OH)_3$ (AR, Sinopharm Chemical Reagent Co., Ltd), colloidal silica (Ludox AS-30, 30%, Grace), and *N*,*N*,*N*-trimethyl-1-adamantyl ammonium hydroxide (TMAdaOH, 25%, Macklin) were used without further purification. Deionized water was obtained from a Master-Q20 ultrapure water system (China Taihe Instruments Co., Ltd). HY zeolite and USY-100 zeolite were purchased from NanHua Catalyst Co., Ltd. The self-made α-Al_2O_3 substrates (20 mm diameter, 2 mm thickness) exhibited approximately 38% porosity.

2.2 Synthesis of low-silica (chabazite) seeds

Low-silica chabazite seeds were prepared *via* the structural transformation of HY zeolite. Specifically, 15 g of HY zeolite was added to 100 g of deionized water and subjected to ball milling for 2 hours to reduce particle size. Subsequently, 3.2683 g of KOH was introduced into the mixture, which was then dispersed by ultrasonication for 30 minutes. The resulting suspension was transferred into a stainless-steel autoclave for hydrothermal crystallization at 100 °C for 48 hours. After the reaction, the synthesized low-silica seeds were collected by centrifugation, washed with deionized water four times, and dried at 100 °C for 40 minutes for further use. The obtained low Si/Al ratio seeds were labeled as C-1.

2.3 Synthesis of high-silica (SSZ-13) seeds

High-silica SSZ-13 seeds were prepared through the structural transformation of USY-100 zeolite. Specifically, 20 g of USY-100 zeolite was added to a mixed solution containing 1.785 g of KOH, 82.23 g of TMAdaOH, and 38.5 g of deionized water. After 30 minutes of ultrasonication, the mixture was transferred into a stainless-steel autoclave for hydrothermal crystallization at 140 °C for 48 hours. The resulting SSZ-13 seeds were collected by centrifugation, washed four times with deionized water, and dried at 100 °C for 40 minutes. Finally, the seeds were calcined at 550 °C for 3 hours in air (heating rate: 10 K min^{-1}) to remove the OSDA. The obtained high Si/Al ratio seeds were designated as S-1.

2.4 Preparation of $KAlO_2$ solution

Since the clear solution is a pure K^+ system, 3.9 g of $Al(OH)_3$ and 5.6 g of KOH were weighed according to a molar ratio of 1 : 2, dissolved in deionized water, and heated to react. The resulting mixture of $KAlO_2$ and KOH was adjusted to a total mass of 50 g and served as the aluminum source.

2.5 Fabrication of CHA zeolite membranes

CHA zeolite membranes were hydrothermally synthesized on α-Al_2O_3 disc-supports *via* a secondary growth method. Specifically, 0.5 g, 1.5 g, and 3.0 g of low-silica or high-silica seeds were separately weighed and dispersed in corresponding amounts of deionized water to prepare 0.5 wt%, 1.5 wt%, and 3.0 wt% seed suspensions. The suspensions were ball-milled for 30 minutes and subsequently stand for 2 hours (see SI videos for specific details). The α-Al_2O_3 supports were then immersed in the seed suspensions for 30 seconds, retrieved, and dried at 80 °C for 2 hours. A clear synthesis solution with a molar composition of $20SiO_2 : 1Al_2O_3 : 15K_2O : 4600H_2O$ was prepared, stirred, and aged at room temperature for 2 hours (See SI for specific details). Place the supports with the seed-coated side facing down, ensuring the other side does not contact the synthesis solution, and perform hydrothermal crystallization at 100–170 °C for 20 hours. The as-synthesized membranes were thoroughly washed with deionized water and dried at 100 °C for 2 hours prior to further use.

2.6 Characterization

The crystal phases of the samples were determined by X-ray diffraction (XRD; Ultima IV, Rigaku) over a 2θ range of 5–80°. The morphology of CHA zeolite particles and membranes was observed using scanning electron microscopy (SEM; ZEISS Sigma 300, Carl Zeiss, Germany). The elemental composition of the seeds and CHA zeolite membranes was analyzed by energy-dispersive X-ray spectroscopy (EDX; EMAX x-act, Horiba).

2.7 PV test

The PV performance of the as-synthesized CHA zeolite membranes was evaluated using a setup schematically illustrated in Fig. 1. A 90 wt% ethanol/water mixture was used as the feed solution, which was circulated through the membrane module *via* a peristaltic pump and then returned to the feed tank. The pump's tubing (excluding the peristaltic section) was wrapped with polyethylene insulation to minimize heat loss from the feed tank to the membrane module, and the feed solution was circulated at a constant flow rate of 20 mL min^{-1} *via* a peristaltic pump to ensure stable hydrodynamic conditions on the membrane surface and mitigate the effects of

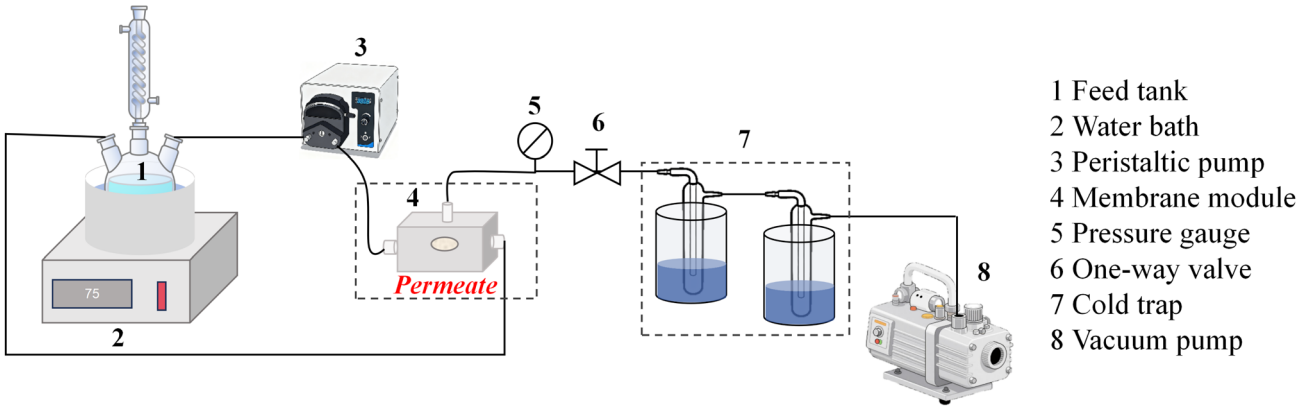

Fig. 1 Schematic diagram of PV test device.

concentration polarization (Table S1). The feed solution was maintained at 75 °C using a water bath, while the membrane module was placed in a 75 °C oven, and the membrane's circumference was sealed with resin, resulting in an effective membrane area of approximately 3 cm^2. The permeate side was continuously evacuated by a vacuum pump to maintain a vacuum level below 100 Pa, and the permeate vapor was collected using a liquid nitrogen cold trap. The compositions of the feed and permeate were analyzed by gas chromatography (GC; GC-7890B, Agilent) equipped with a KB-5 separation column (Kromat Corporation).

The formulas for calculating the permeation flux (J) and separation factor (α) of the membrane are as follows:

$$J = \frac{\omega}{A \cdot \Delta t} \quad (1)$$

$$\alpha = \frac{y_i / y_j}{x_i / x_j} \quad (2)$$

where: ω is the mass of permeate (kg); A is the effective membrane area (m^2); Δt is the sampling time interval (h); x_i and x_j represent the mass fractions of water and ethanol in the feed, respectively; y_i and y_j denote the corresponding mass fractions of water and ethanol in the permeate, respectively.

3. Results and discussion

3.1 Effect of SiO_2/Al_2O_3 ratio of seed

CHA zeolites with different SiO_2/Al_2O_3 ratios were successfully synthesized *via* crystal transformation of Y zeolite. As shown in Fig. 3a, the characteristic diffraction peaks of the obtained samples match well with those in the standard XRD pattern, with no impurity peaks observed, indicating that the as-synthesized CHA zeolites are of high phase purity (Table 1). The low silica-to-alumina ratio seeds (C-1) exhibit a prismatic morphology with crystal sizes of approximately 100–200 nm and a SiO_2/Al_2O_3 ratio of 4.8 (Fig. 2a), while the high silica-to-alumina ratio seeds (S-1) display a cubic morphology with particle sizes of 200–400 nm and a SiO_2/Al_2O_3 ratio of 26.9 (Fig. 2b).

Table 1 SiO_2/Al_2O_3 ratios of seeds and selected membranes

Sample	Chabazite	SSZ-13	M03	M04	M09	M12
SiO_2/Al_2O_3	4.84	26.95	3.66	4.74	5.44	5.29

Seed suspensions with a concentration of 0.5 wt% were prepared from both CHA zeolites mentioned above and applied onto α-Al_2O_3 substrates using dip-coating method to obtain uniform seed layers. The SEM images of the coated supports (Fig. 2c and d) show that, when using C-1 seeds, the particles are distributed in an aggregated manner on the substrate surface. In contrast, the S-1 seeds form a smoother and more uniform coating, which can be attributed to their cubic morphology that facilitates ordered stacking and close packing between adjacent particles. Both types of seed layers evenly cover the substrate without exposing the underlying support.

The XRD patterns of the synthesized CHA membranes are shown in Fig. 3b. The diffraction peaks are in good agreement with the reference pattern, confirming successful membrane formation. Notably, the CHA membrane derived from the low-silica seed exhibits lower peak intensities than that obtained from the high-silica seed, suggesting a difference in crystallinity. This observation is further supported by SEM analysis (Fig. 3c–f). The membrane derived from low-silica seeds consists mainly of stacked pyramidal crystals approximately 2.0 μm in size, with a membrane thickness of about 5.8 μm and small intercrystalline gaps. In contrast, the high-silica seeded membrane is composed of prismatic crystals with sizes around 6 μm and a thickness of approximately 6.4 μm.

The observed difference in crystallinity can be attributed to the distinct dissolution behaviors of the two types of seeds during hydrothermal synthesis. Seed dissolution typically precedes membrane growth: for C-1 seeds, the framework stability is relatively poor, leading to a faster dissolution rate and the rapid generation of numerous primary structural units, which promote dense nucleation and the formation of many small crystallites on the substrate surface. Conversely, the higher framework stability of S-1 seeds results in a slower dissolution rate and fewer nuclei, allowing the silicon and aluminum species in the synthesis solution to preferentially

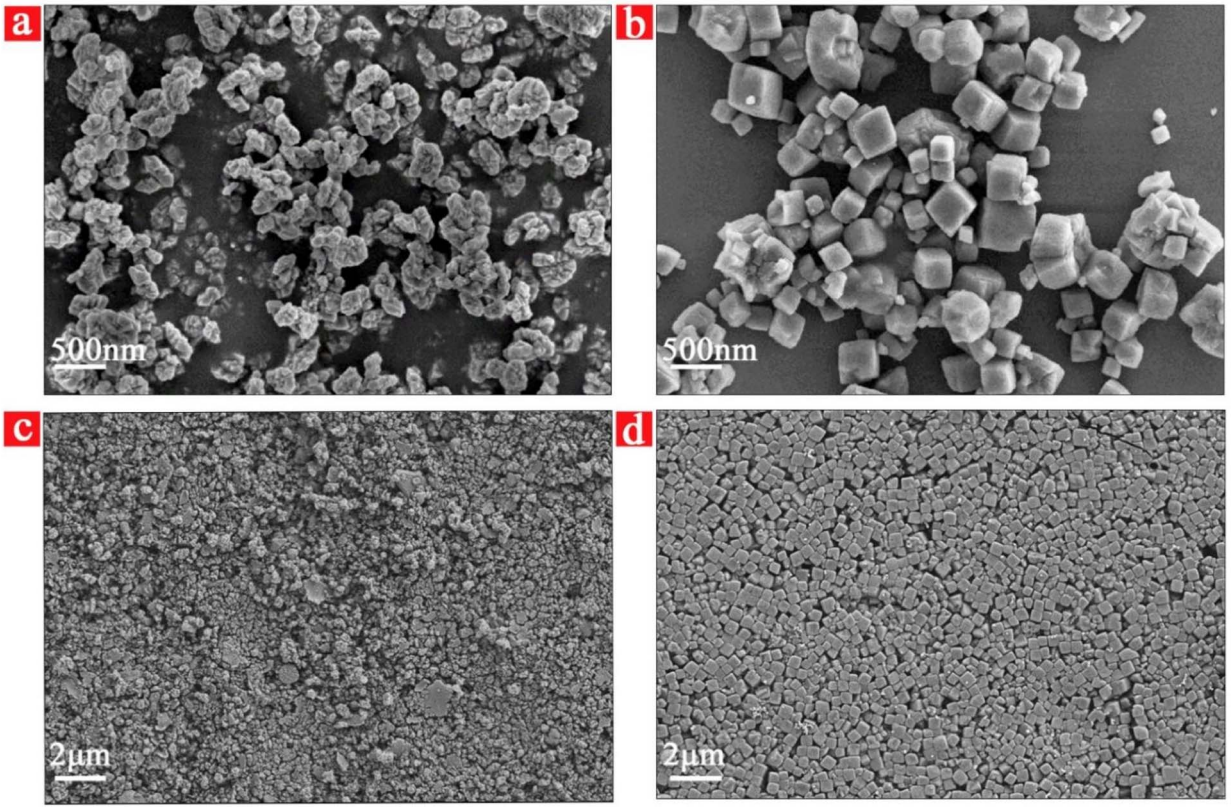

Fig. 2 SEM images of (a) low-silica seeds and (b) high-silica seeds; surface SEM images of the support coated with (c) 0.5 wt% low-silica seeds and (d) 0.5 wt% high-silica seeds.

deposit and grow on existing nuclei, forming larger block-like crystals on the substrate surface.

3.2 Effect of seed concentration on the membrane

Both low- and high-silica seeds could successfully induce the formation of CHA zeolite membranes on α-Al_2O_3 supports. Furthermore, the effect of seed concentration on membrane formation was systematically investigated. As shown in Fig. 4a, when the concentration of low-silica seeds increased from 0.5 wt% to 3.0 wt%, the intensity of the main diffraction peak attributed to the CHA phase gradually increased, indicating enhanced crystallinity. This trend was further confirmed by SEM observations, the cracks are attributed to the difference in thermal expansion coefficients between the film and the carrier during the preparation of SEM samples using liquid nitrogen, leading to differential contraction between the two and consequently forming cracks.[36–38] As shown in Fig. 4c, compared with the membrane synthesized using 0.5 wt% seeds, the sample prepared with 1.5 wt% seeds exhibited larger crystal sizes and more densely packed micron-sized blocky crystals. The intercrystalline gaps nearly disappeared, while the membrane thickness remained almost unchanged. The membrane surface became smoother and more compact, with fewer defects, although a small number of unreacted fine crystals were still observed. When the seed concentration was further increased to 3.0 wt%, well-defined prismatic crystals with sizes of 2–4 μm were formed on the membrane surface, as shown in Fig. 4e. The membrane thickness slightly decreased to approximately 5.4 μm, and the surface became flatter and more uniform, with fewer defects and larger grain sizes. This phenomenon is attributed to the high-density nucleation coverage on the carrier surface when the seed concentration increases to 3.0 wt%. During the early growth stage, crystals rapidly contact each other, shifting the growth pattern from free growth to intense lateral competitive growth and grain boundary fusion. To minimize surface energy, the system promotes crystal growth through an Ostwald ripening mechanism, wherein larger crystals consume smaller crystals or raw materials to grow, preferentially filling lateral voids. This results in significant increases in crystal size, but growth occurs primarily through lateral expansion rather than vertical stacking. Consequently, the film thickness decreases due to compression from the fusion of crystal layers.[39]

For high-silica seeds, the XRD patterns (Fig. 4b) revealed an opposite trend: the intensity of the main CHA peak gradually decreased, accompanied by the emergence of diffraction peaks corresponding to the MER phase. At a concentration of 3.0 wt%, only the characteristic MER diffraction peak at 12.4° was observed, while the CHA peak at 12.8° disappeared, suggesting that the membrane was predominantly composed of MER crystals. This transformation may be due to local compositional deviations in SiO_2/Al_2O_3 ratio at the substrate surface caused by

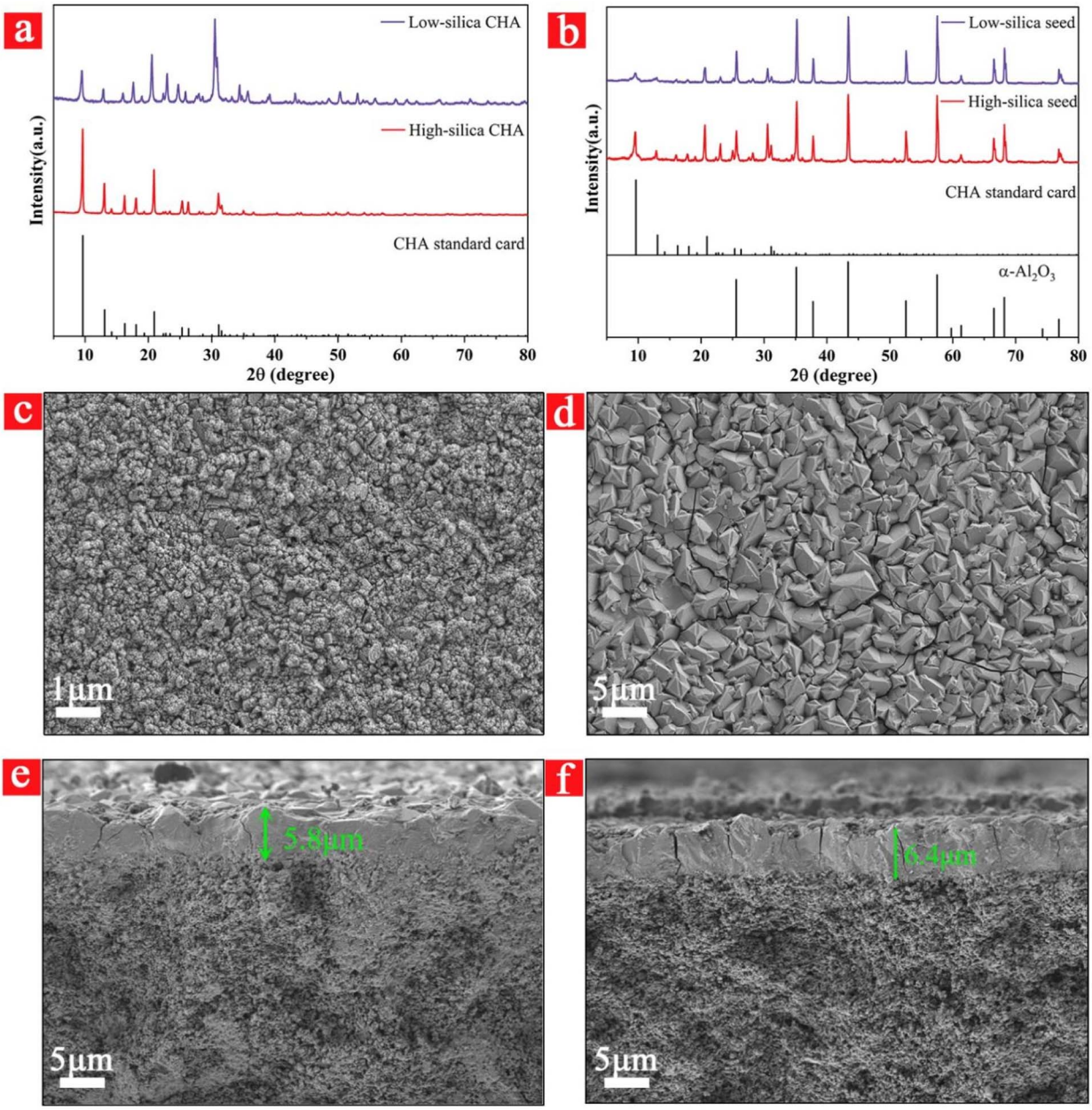

Fig. 3 (a) XRD patterns of low-silica/high-silica seeds and (b) corresponding 0.5 wt% concentration synthesized membranes; (c) SEM image of the surface and (e) cross-section of the CHA zeolite membrane prepared from 0.5 wt% low-silica seeds; (d) SEM image of the surface and (f) cross-section of the CHA zeolite membrane prepared from 0.5 wt% high-silica seeds.

high-silica seed loading, shifting the environment beyond the optimal range for CHA growth and instead favoring MER formation. In some samples without formed membranes, we observed collapse within the cubic crystals of high-silica seeds, revealing voids. However, under these conditions, the dissolved primary units failed to form CHA zeolite membranes (as shown in Fig. S2a). Especially for high-concentration high-silicon seeds, a large number of primary units are dissolved out, which changes the growth environment of CHA zeolite on the surface of the carrier to some extent. Solid XRD results from the mother liquor indicated that as seed concentration increased (Fig. S2b), the main phase distinctly shifted from CHA to MER. corresponding to the emergence of MER crystals in the membrane. This indicates that higher silica seed concentrations indeed favor the formation of MER. When the seed concentration was increased to 1.5 wt%, the membrane surface primarily consisted of CHA crystals with a small amount of coexisting MER phase. Further increasing the concentration to 3.0 wt% led to the frequent appearance of rod-like MER crystals. Given that CHA zeolite has a framework density of 15.1 T/1000 Å^3, while MER has a higher density of 16.4 T/1000 Å^3, the MER phase is thermodynamically more stable. Consequently, a phase transformation from CHA to MER can occur, and such

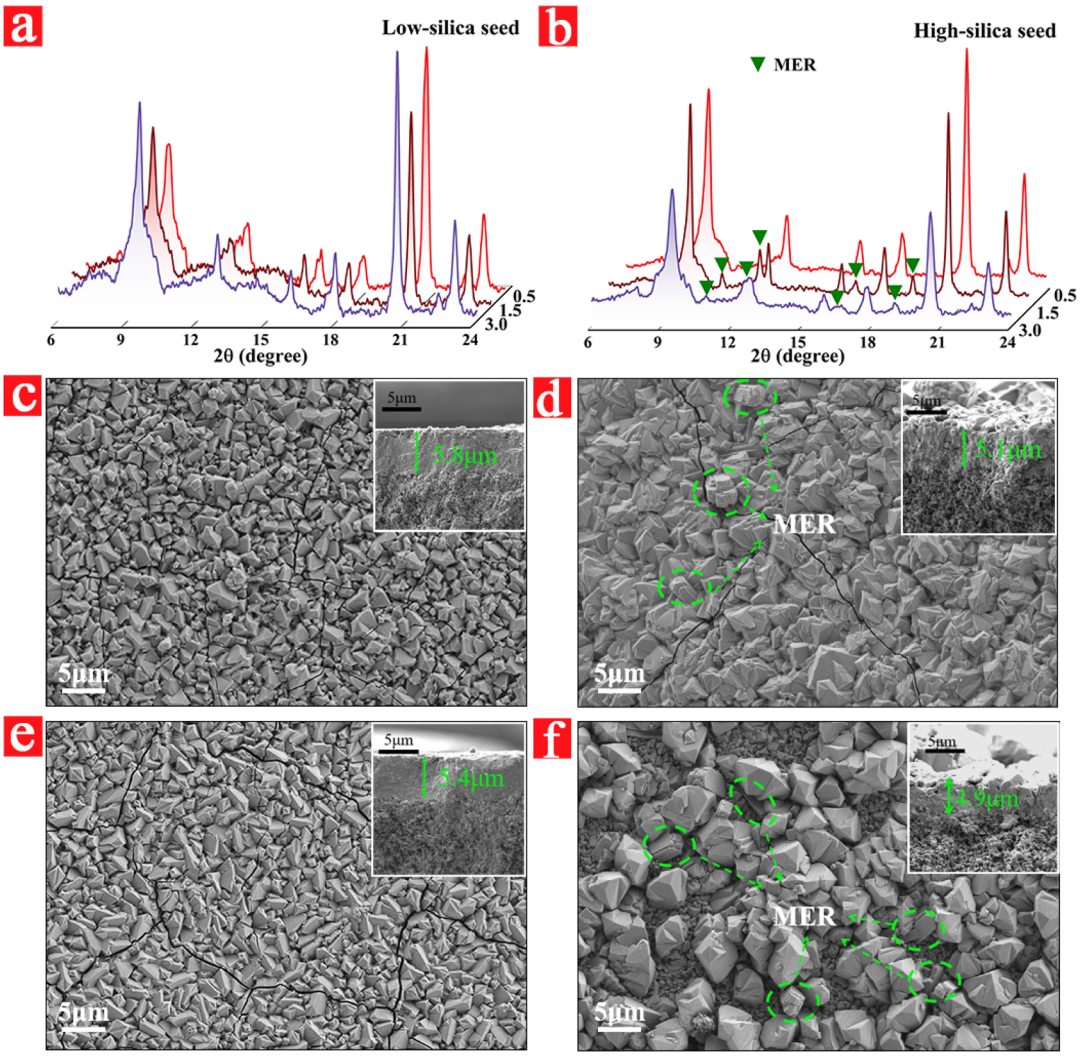

Fig. 4 (a) XRD patterns of CHA zeolite membranes prepared with 0.5 wt%, 1.5 wt%, and 3.0 wt% low-silica seeds, and (b) those prepared with high-silica seeds; SEM images showing surface and cross-sectional views of CHA zeolite membranes synthesized using (c) 1.5 wt% and (e) 3.0 wt% low-silica seeds, and (d) 1.5 wt% and (f) 3.0 wt% high-silica seeds.

transformations between non-topotactic structures have been reported in several previous studies.[40–42]

Therefore, controlling the SiO_2/Al_2O_3 ratio of the seeds is crucial when synthesizing membranes in an OSDA-free, K^+ directed clear-solution system. This may be attributed to changes in the local environment caused by the dissolution of the seed layer, which alters the silica-to-alumina ratio of the synthesis system. A higher silica-to-alumina ratio is more favorable for the growth of MER crystals, thereby making the formation of impurity crystals more likely. Additionally, with increasing high-silica seed concentration, particularly at 3 wt%,a distinct bimodal crystal size distribution was observed on the membrane surface. The lower layer consisted of compact CHA nanocrystals with sizes below 2.5 μm, while the upper layer showed progressively stacked larger crystals. We speculate that the high seed concentration leads to the formation of numerous primary structural units, resulting in abundant small CHA crystals at the bottom. This phenomenon likely results from excessive nucleation due to the high seed loading. At the early stage of synthesis, abundant CHA nanocrystals formed a dense base layer. However, as silicon and aluminum sources were gradually consumed from the synthesis solution, nutrient depletion occurred, and smaller crystals coalesced into larger ones through Ostwald ripening, consistent with the observed reduction in membrane thickness.

3.3 Effect of hydrothermal temperature on membranes

Considering that hydrothermal temperature is a key factor influencing crystal growth, it is essential to investigate its effect on membrane morphology. Based on the previous results, we compared the effects of hydrothermal temperatures of 100 °C, 150 °C, and 170 °C on the growth of CHA zeolite membranes using 3 wt% low-silica seeds and 0.5 wt% high-silica seeds, respectively. The XRD pattern obtained at 100 °C exhibited a weak characteristic CHA peak at 9.8°, along with a broad band between 11° and 21°, which can be attributed to incomplete

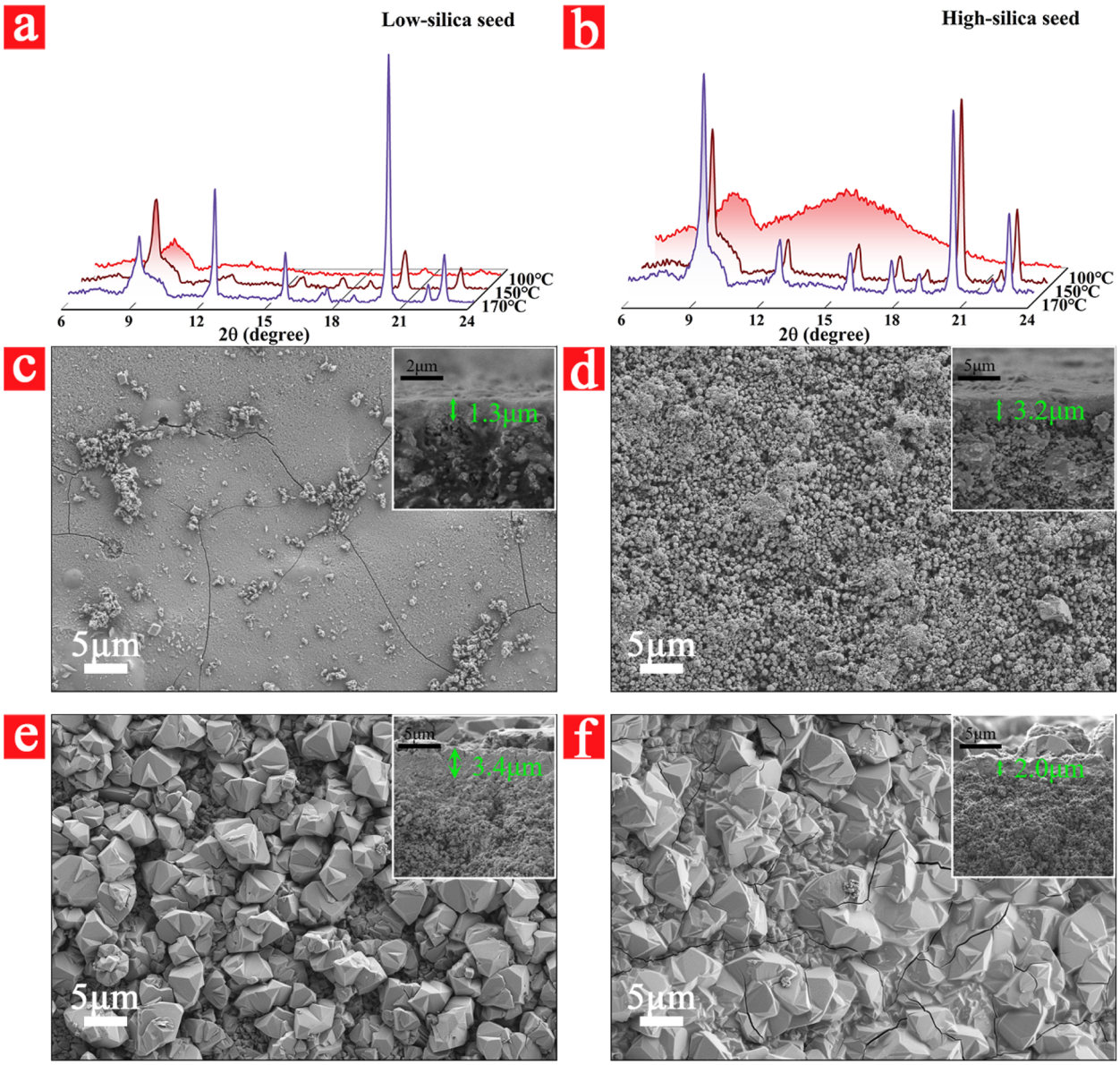

Fig. 5 (a) XRD patterns of CHA zeolite membranes prepared with 3.0 wt% low-silica seeds and (b) 0.5 wt% high-silica seeds at 100–170 °C; SEM images showing surface and cross-sectional views of CHA zeolite membranes synthesized using 3.0 wt% low-silica seeds at (c) 100 °C and (e) 170 °C, and 0.5 wt% high-silica seeds at (d) 100 °C and (f) 170 °C.

crystallization of the CHA membrane at the lower temperature. The weak main peak likely originates from undissolved seed crystals, while the broad band corresponds to amorphous species. This interpretation is supported by the SEM images (Fig. 5c and d): for low-silica seeds, numerous small crystallites are visible on the surface, indicating that the seeds begin to dissolve and transform into primary structural units at 100 °C; in contrast, high-silica seeds display partially dissolved and collapsed cubic crystals.

The incomplete crystallization also resulted in a significant reduction in membrane thickness, measured as 1.3 μm and 3.2 μm for the low- and high-silica seeded samples, respectively. Furthermore, a large amount of amorphous silica was detected in both synthesis gels, suggesting that at 100 °C the silicon source begins to condense but does not yet reach the energy threshold required for crystallization.

Hydrothermal crystallization at 170 °C exerted multiple effects on the membrane derived from 3 wt% low-silica seed coating. Firstly, the elevated temperature accelerated the Ostwald ripening process, promoting the dissolution of small crystals and the further growth of larger ones, leading to crystal coarsening. In addition, this process induced membrane reconstruction, increasing surface defects, reducing smoothness, and causing thickness irregularity, ultimately resulting in an overall thinning of the membrane (Fig. 5e). Meanwhile, the high temperature also favored the formation of secondary phases; locally rod-shaped MER-type crystals were observed in the SEM images (although not clearly detected in the XRD

Table 2 Membrane parameters of M01-M12 and their separation performance for 90 wt% ethanol/water mixture at 75 °C[a]

Membrane	Seed crystal	Seed concentration (wt%)	Temperature (°C)	Thickness (μm)	J (kg m^{-2} h^{-1})	α
M01	Chabazite	0.5	150	~5.8	11.2	2300
M02	Chabazite	1.5	150	~5.8	10.6	3500
M03	Chabazite	3.0	150	~5.4	10.2	5500
M04	SSZ-13	0.5	150	~6.4	9.8	5300
M05	SSZ-13	1.5	150	~5.1	10.4	4100
M06	SSZ-13	3.0	150	~4.9	12.2	1200
M07	Chabazite	3.0	100	~1.3	Leaking	1
M08	Chabazite	3.0	150	~5.2	10.6	5800
M09	Chabazite	3.0	170	~3.4	11.8	1500
M10	SSZ-13	0.5	100	~3.2	Leaking	1
M11	SSZ-13	0.5	150	~6.6	9.5	5400
M12	SSZ-13	0.5	170	~2.0	13.7	2800

[a] The performance data listed in the table are the values recorded after at least 24 hours of continuous operation under steady-state conditions.

patterns), indicating that the conditions had triggered the nucleation of the MER phase.

At 170 °C, the 0.5 wt% high-silica seeded membrane exhibited a morphology distinct from that obtained at 150 °C (Fig. 2d): the crystal edges appeared smooth and fused together, and the membrane thickness decreased to approximately 2 μm (Fig. 5f). This phenomenon can be ascribed to two mechanisms. First, the large number of nuclei formed at high temperature come into contact at an early growth stage, promoting lateral spreading and the formation of a thin continuous layer. Second, the crystallization–dissolution equilibrium at elevated temperature may cause partial crystal dissolution, thereby suppressing vertical membrane growth. Moreover, EDX analysis revealed that the SiO_2/Al_2O_3 ratios of the membranes synthesized from high- and low-silica seeds increased from 4.74 and 3.66 to 5.29 and 5.44, respectively, with increasing temperature, demonstrating that higher hydrothermal temperatures favor the formation of CHA membranes with higher SiO_2/Al_2O_3 ratios.

3.4 PV performance

The PV dehydration performance of the synthesized CHA zeolite membranes was evaluated using a 90 wt% ethanol/water mixture at 75 °C. The separation results are summarized in Table 2. For membranes prepared at 150 °C, as the concentration of low-silica seeds increased, the permeation flux decreased from 11.2 kg m^{-2} h^{-1} to 10.2 kg m^{-2} h^{-1}, while the separation factor increased from 2300 to 5500. This improvement is attributed to enhanced crystal intergrowth on the membrane surface, forming a denser layer composed of bulkier crystals. In the case of high-silica seeds, increasing the seed concentration led to differentiation in CHA zeolite crystal size and the formation of MER zeolite, reducing the actual membrane thickness from approximately 6.4 μm to 4.9 μm. Consequently, although the permeation flux increased from 9.8 kg m^{-2} h^{-1} to

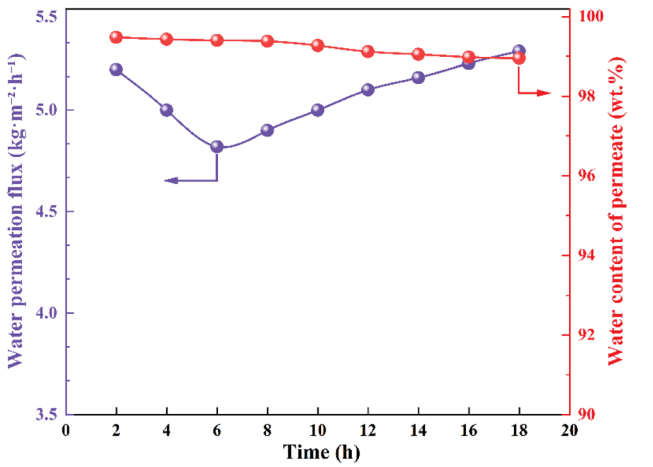

Fig. 6 A PV test was conducted for 18 hours at 75 °C on an M08 experimental 40 wt% acetic acid–water solution.

Table 3 Comparative table of PV performance for CHA zeolite membrane separation of 90 wt% ethanol/water at 75 °C from the literature

SDA	Membrane morphology	Membrane area (cm^2)	J (kg m^{-2} h^{-1})	α	References
Na^+/K^+	Flake crystals	2.83	13.3	6000	12
F^-	Blocky crystals	37.70	5.9	3000	43
Na^+/K^+	Blocky crystals	9.04	6.33	6025	44
Na^+/K^+	Flake crystals	11.3	4.7	>10 000	45
Cs^+/Na^+	Flake crystals	—	1.2	>10 000	46
Cs^+/Na^+	Spherical walnut-shaped crystals	37.70	2.3	3500	10
K^+	Blocky crystals	~3.00	9.8	5800	This work

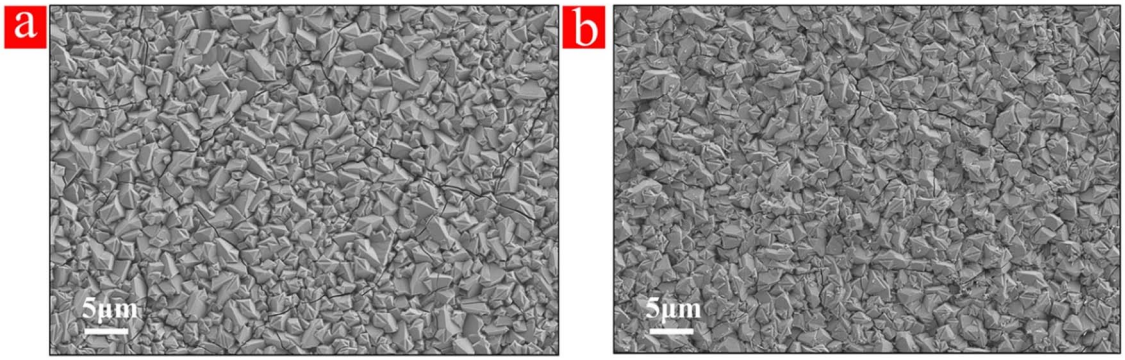

Fig. 7 (a) SEM images of M08 before and (b) after PV testing in acetic acid solution.

12.2 kg m^{-2} h^{-1}, the separation performance deteriorated, with the separation factor decreasing from 5300 to 1200.

At a hydrothermal crystallization temperature of 100 °C, neither the high- nor low-silica seeds formed well-structured CHA zeolite membranes, resulting in direct leakage. When the crystallization temperature was raised to 150 °C, membranes M08 and M03 (prepared with low-silica seeds) as well as M11 and M04 (prepared with high-silica seeds) showed stable permeation flux and separation factor, indicating good reproducibility. At 170 °C, the low-silica seed-derived membranes exhibited differentiation in crystal size and a thinner membrane layer, leading to an increased flux of 11.8 kg m^{-2} h^{-1} but a decreased separation factor of 1500. For the high-silica seed-derived membranes under the same condition, the layer became thinner and partial dissolution of surface crystals was observed, potentially introducing internal defects. This resulted in an increased flux of 13.7 kg m^{-2} h^{-1} and a reduced separation factor of 2800. Based on the overall performance evaluation, the optimal synthesis condition for the CHA zeolite membrane was determined to be 3 wt% low-silica seeds crystallized at 150 °C for 20 h.

Furthermore, we have repeated the clear liquid synthesis of CHA zeolite membrane with the best performance for at least 5 times, and can synthesize pure phase CHA zeolite membrane. Its XRD and PV properties are shown in Fig. S3, XRD spectra indicate that the synthesized CHA zeolite membrane is a pure phase, with permeate flux and separation factor were maintained at about 10.28 ± 0.32 kg m^{-2} h^{-1} and 5560 ± 260, respectively. This demonstrates the excellent reproducibility of synthesizing high-performance CHA zeolite membranes from pure K^+ clear solution. The separation performance of 90wt% ethanol/water PV by CHA zeolite membrane at 75 °C reported in many studies is shown in Table 3. The results show that the transparent clear liquid with single K^+ ion can synthesize CHA zeolite membrane with balanced permeation flux and molecular factor, which shows that this green synthetic CHA zeolite membrane is a synthetic path worthy of further development.

3.5 Acid stability

We conducted an 18 hours PV test on the M08 experimental 40 wt% acetic acid-water solution at 75 °C. The test results are shown in Fig. 6. During the first 6 hours, the water permeation flux decreased from 5.2 kg m^{-2} h^{-1} to 4.8 kg m^{-2} h^{-1} primarily due to competition between strongly polar acetic acid adsorption on the membrane surface and water adsorption, as well as the larger acetic acid molecules (4.4 Å) potentially blocking the CHA zeolite pores (3.8 Å). After 6 hours, the water permeation flux slightly increased, but the water content in the permeate gradually decreased. This was primarily due to the strong acidity dissolving the high-density amorphous phase between crystals or less crystalline CHA zeolite crystals, as well as the selective removal of aluminum from the framework, leading to pore damage. Comparing SEM images of the CHA zeolite membrane before and after acetic acid immersion revealed well-preserved surface morphology (Fig. 7). Although the membrane's performance slightly decreased in acidic conditions, its overall performance remained at a high level. It is important to note that the 18 hours test reflects preliminary operational stability, and longer-term acid stability requires further confirmation.

4. Conclusion

In summary, high-performance CHA zeolite membranes were successfully synthesized using a high water-to-silica ratio (H_2O/SiO_2 = 230) clear solution system, in which K^+ served as the sole structure-directing agent—thus eliminating the need for organic templates. The results demonstrate that the seed type, seed concentration, and crystallization temperature have significant effects on the morphology and PV performance of the CHA membranes. Specifically, membranes synthesized using 3 wt% low-silica seeds or 0.5 wt% high-silica seeds exhibited dense and uniform structures. Low-silica seeds were more effective in suppressing the formation of MER-type impurities, while higher crystallization temperatures led to thinner membrane layers and more defects, resulting in increased permeation flux but reduced separation factors. The membrane synthesized with 3 wt% low-silica seeds at 150 °C (denoted as M08) achieved the best PV performance, with a permeation flux of 10.6 kg m^{-2} h^{-1} and a separation factor of 5800, and showed good repeatability and preliminary acid resistance. Therefore, this study provides valuable theoretical

insights for the green synthesis of high-performance CHA zeolite membranes.

Author contributions

Chuncheng Li: writing-original draft, writing-review &editing, data curation, methodology, resources, funding acquisition. Zijian Zhang: formal analysis, investigation, data curation. Chunwei Yang: writing-review & editing, methodology, validation, data curation, supervision. Pengfei Wang: writing-review & editing, conceptualization, resources, supervision, project administration.

Conflicts of interest

There are no conflicts to declare.

Data availability

The data supporting this article have been included as part of the Supplementary information (SI). Supplementary information is available. See DOI: https://doi.org/10.1039/d6ra00071a.

Acknowledgements

We wish to thank the Shanghai Rising-Star Program (No. 23QB1403900) for financial support through a strategic grant.

References

1 Y. S. Lin and M. C. Duke, Recent progress in polycrystalline zeolite membrane research, *Curr. Opin. Chem. Eng.*, 2013, **2**, 209–216.
2 S. Wang, L. Li, J. Li, J. Wang, E. Pan, J. Lu, Y. Zhang and J. Yang, Sustainable synthesis of highly water-selective ZSM-5 membrane by wet gel conversion, *J. Membr. Sci.*, 2021, **635**, 119431.
3 J. Caro and M. Noack, Zeolite membranes – Recent developments and progress, *Microporous Mesoporous Mater.*, 2008, **115**, 215–233.
4 E. Nagy, P. Mizsey, J. Hancsók, S. Boldyryev and P. Varbanov, Analysis of energy saving by combination of distillation and pervaporation for biofuel production, *Chem. Eng. Process.*, 2015, **98**, 86–94.
5 A. Khalid, M. Aslam, M. A. Qyyum, A. Faisal, A. L. Khan, F. Ahmed, M. Lee, J. Kim, N. Jang, I. S. Chang, A. A. Bazmi and M. Yasin, Membrane separation processes for dehydration of bioethanol from fermentation broths: Recent developments, challenges, and prospects, *Renewable Sustainable Energy Rev.*, 2019, **105**, 427–443.
6 M. Gavahian and A. Farahnaky, Ohmic-assisted hydrodistillation technology: A review, *Trends Food Sci. Technol.*, 2018, **72**, 153–161.
7 P. Shao and R. Y. M. Huang, Polymeric membrane pervaporation, *J. Membr. Sci.*, 2007, **287**, 162–179.
8 L. Jiang, T. Luo, S. Yuan, Y. Wang, X. Xiao, R. Wang, H. Sun, H. Wang, P. Jin and B. Van der Bruggen, Recent Advances in Membrane Synthesis by Interfacial Polymerization for Pervaporation, *Adv. Funct. Mater.*, 2025, **35**, 2500708.
9 M. Sakai, Y. Koshiishi, A. Okada, K. Kawanishi, K. Masuda and M. Matsukata, A Review of Strategies for Developing Zeolite Membranes: From a Microstructure to a Membrane Module, *Cryst. Growth Des.*, 2025, **25**, 5584–5620.
10 Z. Chen, H. Zhang, L. Gan, X. Wu, B. Liu, T. Gui, N. Hu, X. Chen and H. Kita, Hetero-epitaxial growth of chabazite zeolite membranes using an RHO-type seed layer, *J. Membr. Sci.*, 2021, **635**, 119465.
11 N. Hu, Y. Li, S. Zhong, W. Bin, F. Zhang, T. Wu, R. Zhou and X. Chen, Fluoride-mediated synthesis of high-flux chabazite membranes for pervaporation of ethanol using reusable macroporous stainless steel tubes, *J. Membr. Sci.*, 2016, **510**, 91–100.
12 J. Jiang, L. Wang, L. Peng, C. Cai, C. Zhang, X. Wang and X. Gu, Preparation and characterization of high performance CHA zeolite membranes from clear solution, *J. Membr. Sci.*, 2017, **527**, 51–59.
13 R. Tanaka, Y. Ito, Y. Hasegawa and T. Higuchi, Synthesis of LTA zeolite membranes from metal alkoxides and examination of the pervaporation performance, *Microporous Mesoporous Mater.*, 2021, **326**, 111346.
14 B. Liu, H. Kita and K. Yogo, Preparation of Si-rich LTA zeolite membrane using organic template-free solution for methanol dehydration, *Sep. Purif. Technol.*, 2020, **239**, 116533.
15 M. Zhu, S. Huang, Y. Gong, Y. Zhou, X. Chen, Y. Liu, N. Hu, F. Zhang, X. Chen and H. Kita, Effect of flouride on preparation and pervaporation performance of NaY zeolite membrane for EtOH/ETBE mixture, *Microporous Mesoporous Mater.*, 2019, **282**, 48–52.
16 F. Zhang, L. Xu, N. Hu, N. Bu, R. Zhou and X. Chen, Preparation of NaY zeolite membranes in fluoride media and their application in dehydration of bio-alcohols, *Sep. Purif. Technol.*, 2014, **129**, 9–17.
17 M. Ji, X. Gao, X. Wang, Y. Zhang, J. Jiang and X. Gu, An ensemble synthesis strategy for fabrication of hollow fiber T-type zeolite membrane modules, *J. Membr. Sci.*, 2018, **563**, 460–469.
18 L. Li, Y. Lu, L. Li, J. Yang, W. Fu, Y. Luo, J. Lu, Y. Zhang and L. Zhou, Highly selective zeolite T membranes with different ERI stacking faults for pervaporative dehydration of ethanol, *J. Membr. Sci.*, 2021, **638**, 119701.
19 L. Li, J. Li, L. Cheng, J. Wang and J. Yang, Microwave synthesis of high-quality mordenite membrane by a two-stage varying heating-rate procedure, *J. Membr. Sci.*, 2020, **612**, 118479.
20 Y. Li, M. Zhu, N. Hu, F. Zhang, T. Wu, X. Chen and H. Kita, Scale-up of high performance mordenite membranes for dehydration of water-acetic acid mixtures, *J. Membr. Sci.*, 2018, **564**, 174–183.
21 Q. Wang, C. Qian, N. Xu, Q. Liu, B. Wang, L. Zhang, L. Fan and R. Zhou, Synthesis optimization and separation mechanism of ZSM-5 zeolite membranes for pervaporation dehydration of organic solvents, *Sci. Total Environ.*, 2024, **929**, 172641.

22 D. Si, M. Zhu, X. Sun, M. Xue, Y. Li, T. Wu, T. Gui, I. Kumakiri, X. Chen and H. Kita, Formation process and pervaporation of high aluminum ZSM-5 zeolite membrane with fluoride-containing and organic template-free gel, *Sep. Purif. Technol.*, 2021, **257**, 117963.
23 R. Ben Haya, Y. Boucheffa, Z. Ihdene and S. Elbey, Investigation on the residual dehydration capacities of aged industrial LTA molecular sieves, *Microporous Mesoporous Mater.*, 2025, **397**, 113777.
24 J. Jiang, L. Peng, X. Wang, H. Qiu, M. Ji and X. Gu, Effect of Si/Al ratio in the framework on the pervaporation properties of hollow fiber CHA zeolite membranes, *Microporous Mesoporous Mater.*, 2019, **273**, 196–202.
25 A. J. Mallette, K. Shilpa and J. D. Rimer, The Current Understanding of Mechanistic Pathways in Zeolite Crystallization, *Chem. Rev.*, 2024, **124**, 3416–3493.
26 H. Luan, Q. Wu, J. Wu, X. Meng and F.-S. Xiao, Templates for the synthesis of zeolites, *Chin. J. Struct. Chem.*, 2024, **43**, 100252.
27 Y. Wang, Q. Wu, X. Meng and F.-S. Xiao, Insights into the Organotemplate-Free Synthesis of Zeolite Catalysts, *Engineering*, 2017, **3**, 567–574.
28 E. A. Eilertsen, M. Haouas, A. B. Pinar, N. D. Hould, R. F. Lobo, K. P. Lillerud and F. Taulelle, NMR and SAXS Analysis of Connectivity of Aluminum and Silicon Atoms in the Clear Sol Precursor of SSZ-13 Zeolite, *Chem. Mater.*, 2012, **24**, 571–578.
29 X. Kong, H. e. Qiu, Y. Zhang, X. Tang, D. Meng, S. Yang, W. Guo, N. Xu, L. Kong, Y. Zhang and Z. Zhang, Seeded synthesis of all-silica CHA zeolites in diluted mother liquor, *Microporous Mesoporous Mater.*, 2021, **316**, 110914.
30 N. Ma, R. Wang, G. He and Z. Wang, Preparation of high-performance zeolite NaA membranes in clear solution by adding SiO_2 into Al_2O_3 hollow-fiber precursor, *AlChE J.*, 2018, **64**, 2679–2688.
31 X. Zhang, X. Song, L. Qiu, M. Ding, N. Hu, R. Zhou and X. Chen, Synthesis and pervaporation performance of highly reproducible zeolite T membranes from clear solutions, *Chin. J. Catal.*, 2013, **34**, 542–547.
32 I. Kumakiri, T. Yamaguchi and S.-i. Nakao, Preparation of Zeolite A and Faujasite Membranes from a Clear Solution, *Ind. Eng. Chem. Res.*, 1999, **38**, 4682–4688.
33 G. Li, E. Kikuchi and M. Matsukata, ZSM-5 zeolite membranes prepared from a clear template-free solution, *Microporous Mesoporous Mater.*, 2003, **60**, 225–235.
34 T. Wu, Z. Huang, Z. Sun, J. Zeng, Y. Xiao, H. Wu, R. Wu, B. Liu, M. Zhu, F. Zhang, X. Chen and H. Kita, Fluoride-free synthesis of SSZ-13 zeolite membranes from clear-solution with reduced time, *Sep. Purif. Technol.*, 2025, **361**, 131235.
35 L. Li, J. Li, Y. Li, X. Wu, L. Li, W. Zeng, Y. Chen and J. Choi, Sustainable and resource-efficient synthesis of zeolite membranes in a fluoride-free, organic template-free dilute solution, *RSC Adv.*, 2025, **15**, 21859–21871.
36 Y. Hasegawa, C. Abe, M. Nishioka, K. Sato, T. Nagase and T. Hanaoka, Formation of high flux CHA-type zeolite membranes and their application to the dehydration of alcohol solutions, *J. Membr. Sci.*, 2010, **364**, 318–324.
37 R. Zhou, Y. Li, B. Liu, N. Hu, X. Chen and H. Kita, Preparation of chabazite membranes by secondary growth using zeolite-T-directed chabazite seeds, *Microporous Mesoporous Mater.*, 2013, **179**, 128–135.
38 M.-Z. Kim, S. F. Alam, D. Arepalli, A. U. Rehman, W.-Y. Choi and C.-H. Cho, Prevention in Thermal Crack Formation in Chabazite (CHA) Zeolite Membrane by Developing Thin Top Zeolite and Thick Intermediate Layers, *Nanomaterials*, 2021, **11**, 2113.
39 Y. Dong, D. Zhang, D. Li, H. Jia and W. Qin, Control of Ostwald ripening, *Sci. China Mater.*, 2023, **66**, 1249–1255.
40 K. Itabashi, Y. Kamimura, K. Iyoki, A. Shimojima and T. Okubo, A Working Hypothesis for Broadening Framework Types of Zeolites in Seed-Assisted Synthesis without Organic Structure-Directing Agent, *J. Am. Chem. Soc.*, 2012, **134**, 11542–11549.
41 M. Maldonado, M. D. Oleksiak, S. Chinta and J. D. Rimer, Controlling Crystal Polymorphism in Organic-Free Synthesis of Na-Zeolites, *J. Am. Chem. Soc.*, 2013, **135**, 2641–2652.
42 G. T. M. Kadja, I. R. Kadir, A. T. N. Fajar, V. Suendo and R. R. Mukti, Revisiting the seed-assisted synthesis of zeolites without organic structure-directing agents: insights from the CHA case, *RSC Adv.*, 2020, **10**, 5304–5315.
43 B. Zhu, Y. Li, Z. Yan, Z. Yang, X. Wu, T. Gui, Y. Li, F. Zhang, X. Chen and H. Kita, Formation process of organic template-free chabazite zeolite membrane and its separation performance of water-rich mixtures, *Microporous Mesoporous Mater.*, 2022, **341**, 112085.
44 Y. Qian, T. Ma, Z. Lu, Z. Yang, G. Dai, R. Song, J. Jiang, X. Wang and X. Gu, Template-free synthesis of CHA zeolite membranes with improved stability using exotic KFI zeolite seeds, *J. Membr. Sci.*, 2026, **742**, 125119.
45 L. Li, X. Liu, Z. R. Gao, Z. Gao, P. Wan, W. Yan, G. He, C. He, J. Yang and M. Tsapatsis, Intensified Heterogeneous Growth of High-Performance CHA Membranes from Hierarchical Zeolite T Seeds, *Adv. Funct. Mater.*, 2025, **35**, e11555.
46 J. Du, J. Jiang, Z. Xue, Y. Hu, B. Liu, R. Zhou and W. Xing, Template-Free Synthesis of High Dehydration Performance CHA Zeolite Membranes with Increased Si/Al Ratio Using SSZ-13 Seeds, *Membranes*, 2024, **14**, 78.